Applied Physics Letters

RESEARCH ARTICLE | APRIL 10 2023

Effects of temperature and DC cycling stress on resistive switching mechanisms in hafnia-based ferroelectric tunnel junction

Special Collection: Electronic Noise: From Advanced Materials to Quantum Technologies

Wonjun Shin; Ryun-Han Koo; Kyung Kyu Min; ... et. al

Appl. Phys. Lett. 122, 152901 (2023)
https://doi.org/10.1063/5.0140954

CrossMark

Articles You May Be Interested In

Understanding tunneling electroresistance effect through potential profile in Pt/$Hf_{0.5}Zr_{0.5}O_2$/TiN ferroelectric tunnel junction memory

Appl. Phys. Lett. (October 2019)

A method of controlling the imprint effect in hafnia ferroelectric device

Appl. Phys. Lett. (January 2023)

Ultra-thin $Hf_{0.5}Zr_{0.5}O_2$ thin-film-based ferroelectric tunnel junction via stress induced crystallization

Appl. Phys. Lett. (December 2020)

Downloaded from http://pubs.aip.org/aip/apl/article-pdf/doi/10.1063/5.0140954/16821168/152901_1_5.0140954.pdf

Effects of temperature and DC cycling stress on resistive switching mechanisms in hafnia-based ferroelectric tunnel junction

Cite as: Appl. Phys. Lett. **122**, 152901 (2023); doi: 10.1063/5.0140954
Submitted: 1 January 2023 · Accepted: 25 March 2023 ·
Published Online: 10 April 2023

View Online

Export Citation

CrossMark

Wonjun Shin,[1] Ryun-Han Koo,[1] Kyung Kyu Min,[1] Been Kwak,[2] Dongseok Kwon,[1] Daewoong Kwon,[2,a)] and Jong-Ho Lee[1,3,a)]

AFFILIATIONS

[1]Inter-University Semiconductor Research Center, Department of Electrical and Computer Engineering, Seoul National University, Seoul 08826, South Korea
[2]Department of Electronic Engineering, Hanyang University, Seoul 04763, South Korea
[3]Ministry of Science and ICT, Sejong 30121, Republic of Korea

Note: This paper is part of the APL Special Collection on Electronic Noise: From Advanced Materials to Quantum Technologies.
[a)]**Authors to whom correspondence should be addressed:** dk79kwon@hanyang.ac.kr and jhl@snu.ac.kr

ABSTRACT

We propose an accurate and effective method, low-frequency noise (LFN) spectroscopy, to examine the resistive switching mechanism in ferroelectric tunnel junctions (FTJs) based on pure hafnium oxide (HfO_x). Contrary to previous studies that primarily focused on the ferroelectric (FE) resistive switching (RS) in HfO_x-based FTJs, the results of this study demonstrate that non-FE RS affected by the redistribution of oxygen vacancies also plays a significant role in determining the performance of FTJs. LFN spectroscopy is conducted in different conditions by changing the operating temperature and inducing DC cycling stress. The results reveal that the RS mechanism changes from FE to non-FE RS with increased program bias in all conditions. This change is facilitated by the rise in temperature and the number of DC cycling stress.

Published under an exclusive license by AIP Publishing. https://doi.org/10.1063/5.0140954

The concept of integrating ferroelectricity into memory technology has a lengthy history, originating in 1957.[1] The original idea was to develop a device that could switch and store information in a nonvolatile manner that could be read nondestructively. Since then, considerable attempts have been directed toward commercializing ferroelectric (FE)-based memories, such as FE field-effect transistors (FEFETs).[2–4] The most widely investigated FE material has been perovskites, including lead zirconate titanate (PZT)[5] and strontium bismuth tantalate (SBT),[6] and they demonstrated highly promising memory performance. Perovskite materials, however, are incompatible with conventional complementary metal-oxide-semiconductor (CMOS) technology and have a scaling limitation because their thickness must exceed 100 nm to induce ferroelectricity.[7] As a result, the commercialization of perovskite-based FEFETs failed in competition with charge trap-based FETs in the memory industry.

In 2011, the discovery of ferroelectricity in hafnia-based materials paved a new possibility for ferroelectric-based memories.[8] Boscke *et al.* reported that a crystalline phase with ferroelectric behavior could be formed by doping silicon oxide (SiO_2) into hafnium oxide (HfO_x) films.[8] Contrary to perovskite materials, since 2007, HfO_x has been used as the gate dielectric in 45 nm high-k MOSFET posing perfect CMOS compatibility.[9] Furthermore, Cheema *et al.* reported that ferroelectricity could be realized in HfO_x as thin as 1 nm, thereby resolving the scaling limitation of perovskite materials.[10] Thus, extensive studies have attempted to fully realize the potential of HfOx-based FE memory devices.

Among different types of FE-based memory devices, the FE tunnel junctions (FTJs) are advantageous owing to their ease of fabrication and high scalability.[11,12] FTJs have a structure wherein the FE material is sandwiched between the top electrode (TE) and the bottom electrode (BE). The magnitude of tunneling electroresistance (TER) changes with the polarization direction of the FE layer, which can be controlled by the program bias (V_{PGM}). Additionally, FTJs have recently been integrated into neuromorphic computing as synaptic devices using the partial polarization of the FE material.[13]

Published under an exclusive license by AIP Publishing

Downloaded from http://pubs.aip.org/aip/apl/article-pdf/doi/10.1063/5.0140954/16821168/152901_1_5.0140954.pdf

To improve the performance of FTJs, previous studies have primarily focused on increasing the remnant polarization (P_r), decreasing the coercive voltage (V_C), and improving the switching speed of FE materials.[14–16] Evidently, the focus of past research has been advancing the FE properties of HfO_x materials. However, recent studies have demonstrated that the operating principle of HfO_x-based FTJs is not influenced by FE resistive switching (RS) alone and that it is also influenced by non-FE RS, such as oxygen vacancy redistribution or the formation of conduction filament.[17–19] Therefore, it is crucial to consider both the FE RS and non-FE RS optimizing the performance of FTJs. To perform such an optimization, a method of distinguishing the FE and non-FE RS is required. Mikheev *et al.* distinguished the different RS mechanisms inherent to FTJs by investigating the current–voltage characterization, wake-up behavior of the TER ratio, a correlation between RS voltage and V_C, and temperature dependence of both TER ratio and RS voltage.[18] Although different RS mechanisms can be distinguished using the proposed method, it has the limitation of a complicated measurement scheme and process. Therefore, an alternative method is required to examine the RS mechanisms in FTJs.

Low-frequency noise (LFN) spectroscopy has been widely used to examine the operating principle of electronic devices.[19–21] Owing to its sensitivity to traps and impurities in electronic materials, the investigation of LFN provides valuable insights into the conduction process of electronic devices. It has been reported that LFN exhibits much higher sensitivity to a change in conduction mechanism compared to other DC measurements. LFN spectroscopy can be used to investigate the conduction and RS mechanisms of the FTJs[21,22] and obtain essential information on different RS mechanisms intrinsic to FTJs.

In this study, we perform an accurate analysis of both FE and non-FE RS mechanisms by examining the effects of V_{PGM} on the LFN characteristics of FTJs under different conditions: change in temperature (T) and DC cycling stress. The metal-FE-dielectric (DE) (insulator)–semiconductor (MFIS) stack is used as a structure of the FTJ, and pure HfO_x is used as a FE material. It is revealed that the FE and non-FE RS mechanisms can be accurately distinguished using LFN spectroscopy.

Figure 1(a) illustrates the schematic cross section view of the fabricated FTJ. The corresponding fabrication process is described in Fig. 1(b). A SiO_2 layer is formed via chemical oxidation with an ammonia-peroxide mixture solution. The HfO_x layer was deposited via atomic layer deposition (ALD) using tetrakis hafnium and ozone as a Hf precursor and oxidant, respectively. TiN was deposited via the sputtering process. In order to create an o-phase in pure HfO_x, HfO_x is subjected to rapid thermal annealing. Because of the differing thermal expansion coefficients of TiN, HfO_x, and Si, thermal expansion/contraction during a rise/fall in temperature causes tensile stress in the HfO_x layer. Specifically, the rapid dropping rate of RTA (8.3 s/100 °C) during the cooling process generates stress that leads to the formation of an o-phase in HfO_x. Note that the post-metal annealing was conducted at 800 °C to induce ferroelectricity in the HfO_x. Figures 1(c) and 1(d) correspondingly display a transmission electron microscopy (TEM) cross-sectional image and grazing incidence x-ray diffraction (GIXRD) analysis of the fabricated FTJ. The orthorhombic phase (o-phase) that generates ferroelectricity in HfO_x is evident. The width (W) and length (L) of the top gate are 100 μm.

First, the RS mechanism of the fabricated FTJs is investigated for varying values of T. Figure 2(a) depicts the tunneling current (I_T) density (I_T/WL) vs voltage (V) applied to TiN as a parameter of T.

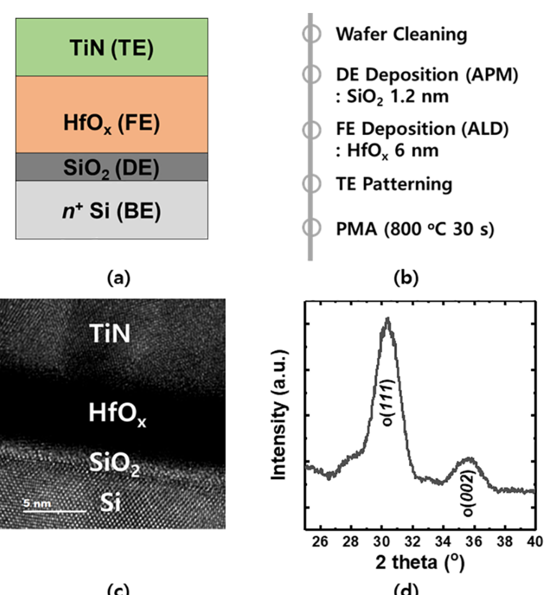

FIG. 1. (a) Schematic cross section and (b) fabrication process of the FTJ. (c) Transmission electron microscopy (TEM) cross-sectional image and (d) grazing incidence x-ray diffraction (GIXRD) analysis of the fabricated FTJ.

Figure 2(b) illustrates polarization vs V curves of the fabricated FTJ measured at various T values. A slight increase in P_r and a decrease in V_C can be observed as T increases. This is because the increase in T facilitates the oxygen vacancy redistribution from the interface between the TiN and HfO_x to the bulk of HfO_x. It has been reported that the oxygen vacancy at the interface pins the ferroelectric dipole of HfO_x and reduces the magnitude of polarization.[23] However, when T is raised and oxygen vacancies are migrated to the bulk of HfO_x, the polarization increases.[23] To investigate the effects of T on FE and non-FE RS, the dependence of I_T on V_{PGM} and T is investigated [Fig. 2(c)]. For all values of Ts, an increase in I_T is observed as V_{PGM} increases. Note that the T_{PGM} is 10 μs. However, it is difficult to examine the exact RS mechanism and distinguish the FE and non-FE RS only with this information.

To demonstrate the effects of T on RS of FTJs, the power spectral density (PSD) is measured at various values of T (40, 60, 80, and 100 °C) as V_{PGM} changes. Figures 3(a)–3(d) show tunneling current normalized PSD S_{IT}/I_T^2 of the FTJs vs f as a parameter of V_{PGM} at 40, 60, 80, and 100 °C, respectively. The read bias (V_{READ}) for PSD measurement is fixed at 2.0 V. The PSD of the FTJ in the high resistance state (HRS) is represented as a reference. In all cases, the FTJs exhibit $1/f^{\gamma}$ [$\gamma = -\ln(S_{IT})/\ln f$] noise behavior. In general, $1/f$ noise originates from the capture/emission of carriers to/from defects. The γ value of the FTJs is close to one regardless of V_{PGM}, demonstrating the high defect density of HfO_x. For all values of T, the S_{IT}/I_T^2 increases with an increase in V_{PGM} for certain V_{PGM} (40 °C: 4.1 V, 60 °C: 4.0 V, 80 °C: 3.95 V, and 40 °C: 3.85 V) as shown in Figs. 3(a-1)–3(d-1). However, the S_{IT}/I_T^2 decreases with a further increase in V_{PGM} as shown in Figs. 3(a-2)–3(d-2). The change in the dependence of S_{IT}/I_T^2 on V_{PGM} demonstrates that the conduction mechanism of FTJs is changed with V_{PGM}.

The $1/f$ noise behavior in the low V_{PGM} region can be explained by the FE RS mechanism. When the conduction of FTJs is governed

Downloaded from http://pubs.aip.org/aip/apl/article-pdf/doi/10.1063/5.0140954/16821168/152901_1_5.0140954.pdf

Published under an exclusive license by AIP Publishing

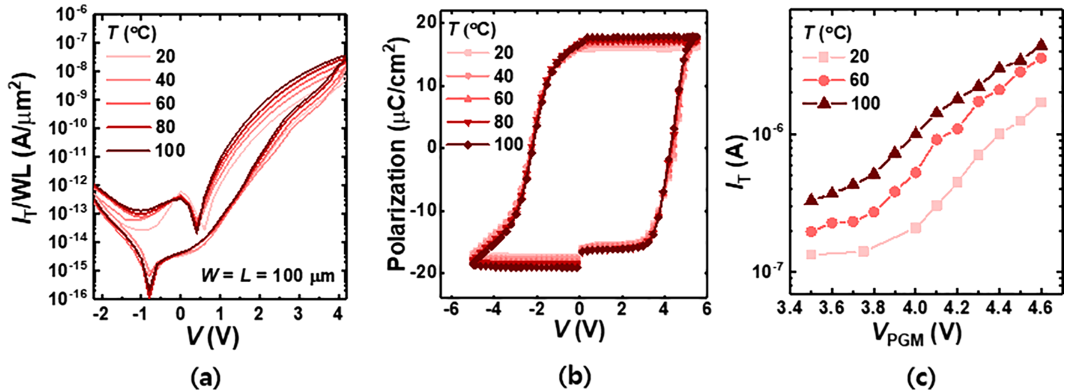

FIG. 2. (a) Tunneling current density (I_T/WL) vs voltage (V) applied to TiN. (b) Polarization vs V curves of the fabricated FTJ measured at various values of T (20, 40, 60, 80, and 100 °C). (c) I_T vs V_{PGM} (from 3.5 to 4.6 V) as a parameter of T.

by FE RS, the carrier transport is primarily determined by Poole–Frenkel (PF) emission.[21] Fowler–Nordheim (FN) tunneling is excluded as a dominant conduction mechanism because the I_T of the FTJs exhibits a strong dependence on T [Fig. 2(a)]. When the $1/f$ noise is generated from the PF emission, S_{IT}/I_T^2 is expressed as follows:[24]

$$\frac{S_{IT}}{I_T{}^2} = \frac{\beta^2 N_D}{E\epsilon_{ins}{}^2 WL}\frac{q^2 A}{f}, \tag{1}$$

where β denotes the fitting parameter, N_D indicates the trap density, E denotes the electric field, ϵ_{ins} symbolizes the permittivity of the

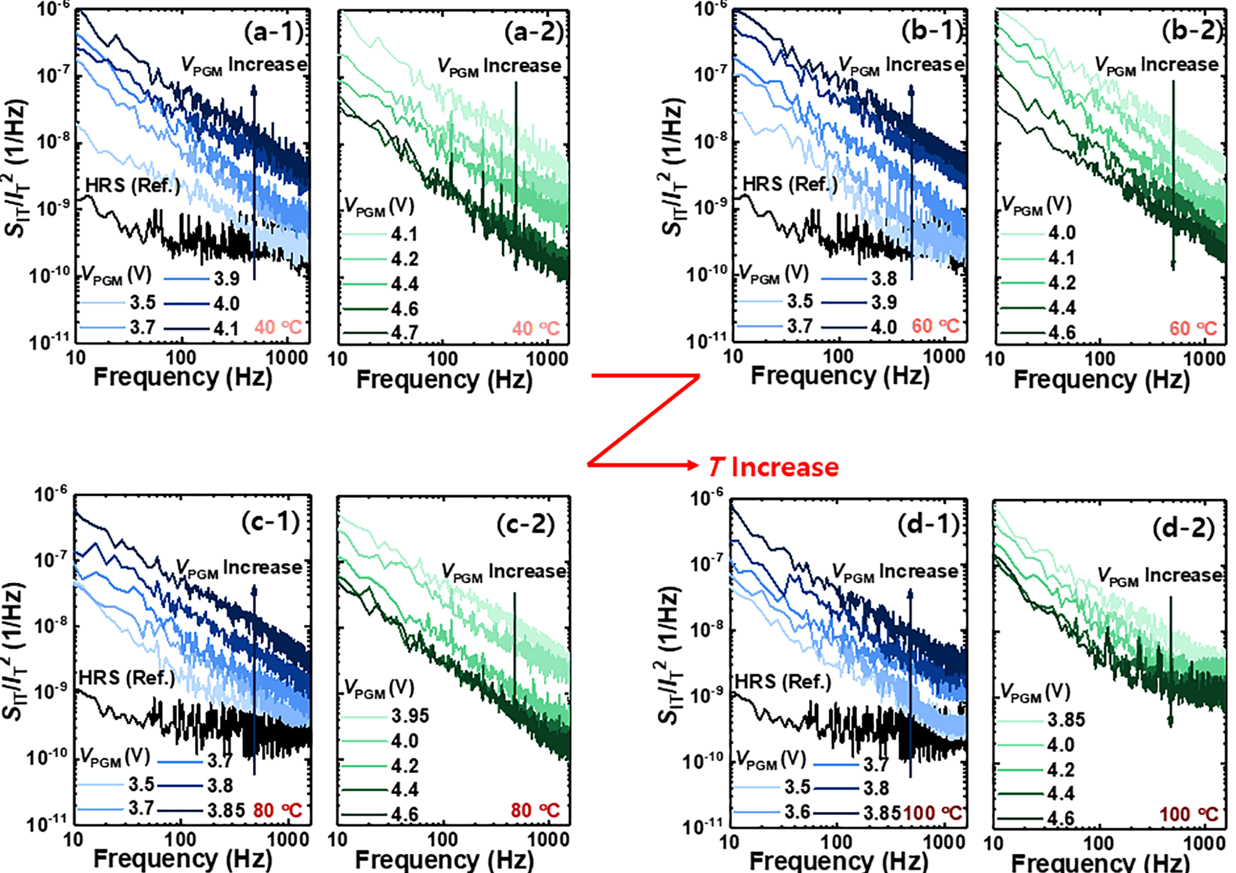

FIG. 3. S_{IT}/I_T^2 of the FTJs vs frequency measured by varying V_{PGM} under T = (a) 40, (b) 60, (c) 80, and (d) 100 °C.

Published under an exclusive license by AIP Publishing

Downloaded from http://pubs.aip.org/aip/apl/article-pdf/doi/10.1063/5.0140954/16821168/152901_1_5.0140954.pdf

insulator layer, and A denotes the ratio of trap time constants, respectively. When V_{PGM} is applied to TiN, P_r induces an E field in the Si–TiN direction in the HfO_x layer and in the TiN–Si direction in SiO_2 and Si layers. With an increase in V_{PGM}, the increased P_r induces a larger E field in Si, resulting in additional electrons tunneling into the HfO_x layer. In the read operation, positive V_{READ} applied to TiN induces the E field in HfO_x, whose direction is opposite to that caused by P_r. Therefore, the E field in HfO_x that governs the PF emission decreases with an increase in V_{PGM}, increasing S_{IT}/I_T^2, as illustrated in Figs. 3(a-1)–3(d-1).

In contrast, the $1/f$ noise behavior in the high V_{PGM} region can be explained by the non-FE RS mechanism. When a large V_{PGM} is applied to TiN, the oxygen vacancy in HfO_x migrates from the TE/FE interface to the FE/DE interface, thereby decreasing the barrier height at the FE/DE interface. With an increase in V_{PGM}, S_{IT}/I_T^2 decreases as the barrier height is decreased by the accumulated oxygen vacancy,[25] as illustrated in Figs. 3(a-1)–3(d-1). As shown in Fig. 2(c), the switching of the FTJ occurs in the program time of μs range. The electronic conduction in oxides is of order of 1 $cm^2/V\,s^{-1}$, corresponding to a timescale of $\sim$ 1 ps. Thus, the electronic conduction cannot explain the μs range switching behavior of the FTJs programmed at a high V_{PGM}. Rather the oxygen vacancy redistribution, whose operating timescale is in μs range,[26] describes the behavior of FTJs.

Figure 4(a) shows the schematic energy band diagram of the FTJs when different values of V_{PGM} are applied to the TiN ($V_{READ} = 0$ V). The energy band diagram is illustrated in three cases based on the V_{PGM} in which the transition of RS occurs (V_{TRANS}). The dotted, dashed, and solid lines represent the case when the V_{PGM} is much smaller than V_{TRANS}, slightly smaller than V_{TRANS}, and larger than V_{TRANS}, respectively. During the read period, the V_{PGM} is smaller than V_{TRANS} and PF emission predominantly constitutes the conduction process. In this case, a larger V_{PGM} decreases E in the HfO_x, resulting in an increase in S_{IT}/I_T^2 [process (1) in Fig. 4(b)]. However, as V_{PGM} exceeds V_{TRANS}, the PF emission no longer governs the conduction, and the Schottky emission governed by barrier height at the FE/DE interface begins to dominate the conduction mechanism of the FTJs [process (2) in Fig. 4(b)].

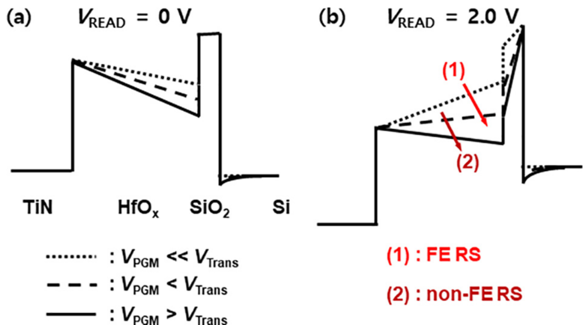

FIG. 4. Schematic energy band diagram of the FTJs when different values of V_{PGM} are applied to TiN [(a): $V_{READ} = 0$ and (b): $V_{READ} = 2.0$ V]. The energy band diagram is illustrated for three cases based on V_{TRANS}. The dotted, dashed, and solid lines represent the case when the V_{PGM} is much smaller than V_{TRANS}, slightly smaller than V_{TRANS}, and larger than V_{TRANS}, respectively. The carrier transport mechanisms of the FTJs are governed by PF emission/Schottky emission when the V_{PGM} is smaller/larger than V_{TRANS}, respectively.

Figure 5 shows the S_{IT}/I_T^2 sampled at 100 Hz vs V_{PGM} as a parameter of T. The V_{TRANS} is clearly observed for all values of T. Interestingly, V_{TRANS} decreases with an increase in T. Because P_r and E_c are almost unchanged by T [Fig. 2(b)], such a change in V_{TRANS} is affected by the non-FE RS characteristics. For a higher T, the redistribution of the oxygen vacancy in the HfO_x film is facilitated because the mobility of oxygen vacancy is increased.[23] Therefore, V_{TRANS} is decreased at a higher T. These results demonstrate that LFN spectroscopy can effectively distinguish the two different RS mechanisms inherent to FTJs by simply investigating the dependence of S_{IT}/I_T^2 on V_{PGM}. The proposed method has merit in terms of ease of measurement and identification compared to the method reported by Mikheev *et al.*[18]

Furthermore, we investigate the effects of DC cycling damage on the RS mechanism of FTJs. Figure 6(a) shows the $|I_T|$ vs V with an increase in the number (N) of DC cycling. DC cycling is applied ten times to FTJs with a V range from -2.0 to 4.5 V. The I_T value of the FTJ increases in both HRS and low-resistance state (LRS) with DC cycling stress. To find the origin of such an increase, the ferroelectricity of the FTJs is investigated. Figure 6(b) shows the polarization vs V curves of the FTJs in the pristine and damaged states. A decrease in P_r of FTJs is observed in the damaged device. When excessive N is applied to the device, oxygen vacancies are generated at the TiN/HfO_x interface. Such defects cause charge trapping, increasing the field over the interface and, accordingly, decreasing the field inside the HfO_x. At the same time, the trapped charges generate dipoles that impede the switching of the domains, resulting in pinning of the domains. Therefore, the magnitude of polarization is decreased.

Figures 6(c) and 6(d) correspondingly show the measured I_T of FTJ in HRS ($I_{T,HRS}$) and LRS ($I_{T,LRS}$) vs N at two different V_{READ} values. As DC cycling stress is applied, I_T of the device in HRS increases, while that in LRS exhibits a slight increase. Note that the steep increase in the $I_{T,HRS}$ is observed at the initial stage of N in Fig. 6(c). This increase originates from the soft breakdown of the HfO_x. It has been reported that the resistance of the HfO_x-based films is significantly decreased due to the soft breakdown caused by the initial program bias.[27] Previous studies have reported that when the FE RS governs the conduction of FTJs, the carrier transport is dominated by trap-assisted tunneling (interface-limited) and PF emission (bulk-limited) in the

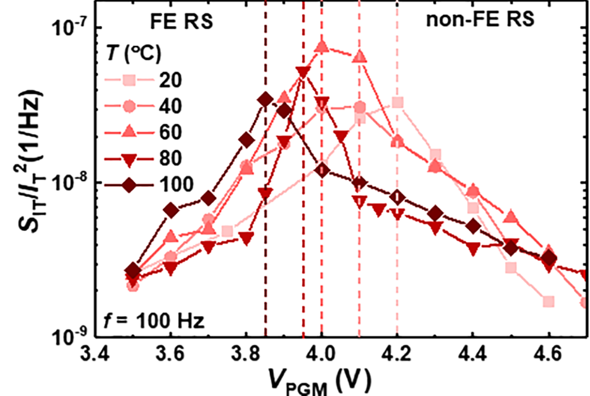

FIG. 5. S_{IT}/I_T^2 sampled at 100 Hz vs V_{PGM} as a parameter of T (20, 60, and 100 °C).

Downloaded from http://pubs.aip.org/aip/apl/article-pdf/doi/10.1063/5.0140954/16821168/152901_1_5.0140954.pdf

Published under an exclusive license by AIP Publishing

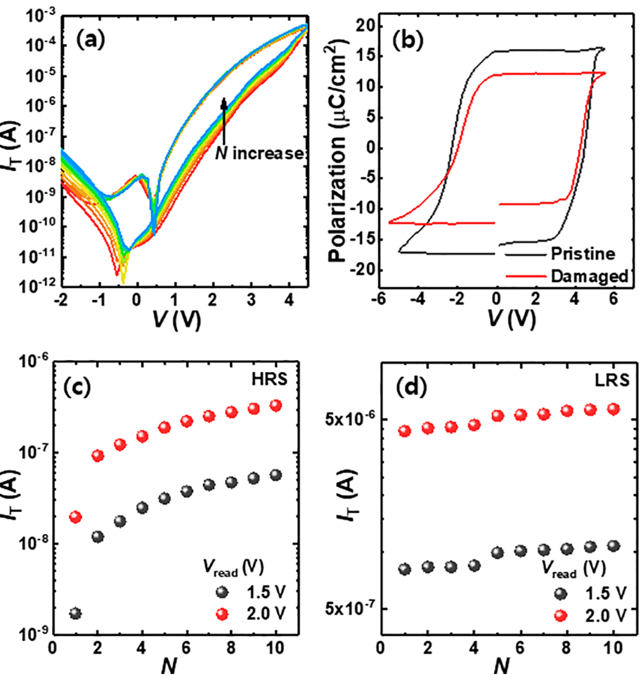

FIG. 6. (a) $|I_T|$ vs V with an increase in the N up to 10 times. (b) Polarization vs V curves of the FTJs in the pristine and damaged states (after ten times double sweep). Measured I_T of FTJ in HRS (c) and LRS (d) vs N at two different V_{read} (1.5 and 2.0 V).

HRS and the LRS, respectively.[21] The increase in I_T in HRS induced by DC cycling stress can be explained by a decrease in P_r and an increase in the interface traps between FE and DE. However, the decreases in P_r cannot explain the damage-induced I_T increase in LRS. If only FE RS is considered, the decrease in P_r should decrease I_T of the FTJ operating in the LRS. Therefore, factors other than FE RS should be considered when explaining the increase in I_T. There are two possible scenarios to explain this phenomenon: First, the damage increases the bulk trap density of HfO_x, increasing the PF emission. Second, DC cycling-induced damage makes that oxygen vacancies migrate more easily, promoting the non-FE RS. Table I summarizes possible scenarios to explain the trend in I_T of the damaged device.

LFN spectroscopy is used to verify which scenario is true. Figure 7(a) shows S_{IT}/I_T^2 of the damaged FTJs vs f as a parameter of

TABLE I. Summary of possible scenarios to explain the trend in I_T of the damaged device.

	HRS (interface limited)	LRS (bulk limited)
P_R decrease	↑	↓
Interface trap increase	↑	⋯
SCE 1: Bulk trap increase	⋯	↑
SCE2: Mobility of oxygen vacancy increase	⋯	↑
Result	↑↑	↑

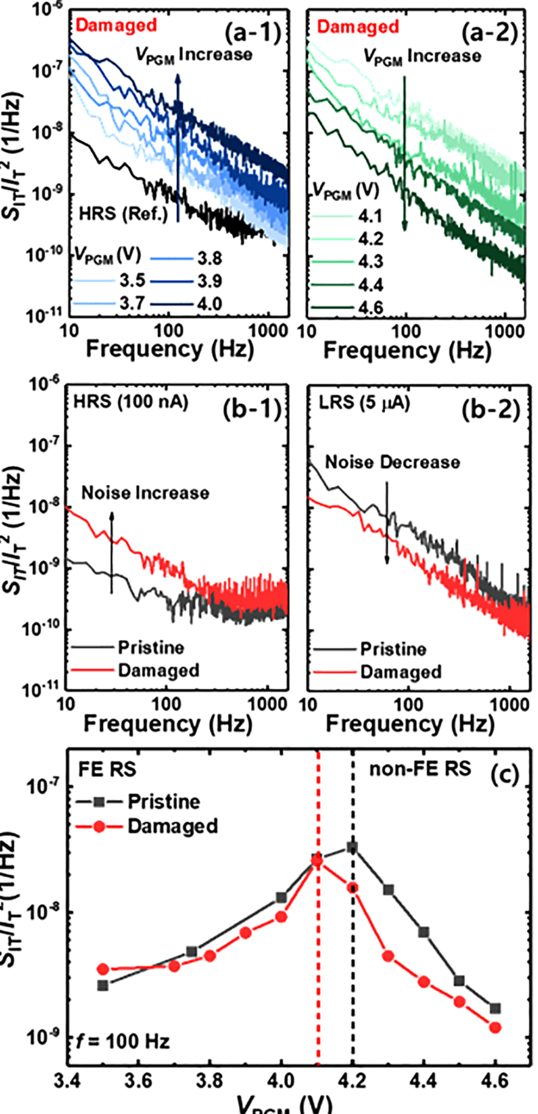

FIG. 7. S_{IT}/I_T^2 of the damaged FTJs vs f as a parameter of V_{PGM} [3.5–4.0 V in (a-1), 4.1–4.6 V in (a-2)]. S_{IT}/I_T^2 vs f of the pristine and damaged FTJs operating in the HRS (b-1) and LRS (b-2). (c) S_{IT}/I_T^2 sampled at 100 Hz vs V_{PGM} of the pristine and damaged FTJs. V_{TRANS} of the damaged FTJs (4.1 V) is lower than that of pristine devices (4.2 V).

V_{PGM}. A similar tendency to that shown in Fig. 3 is observed. In lower V_{PGM}, S_{IT}/I_T^2 increases as V_{PGM} increases because of partial FE domain switching [Fig. 7(a-1)]. In higher V_{PGM}, S_{IT}/I_T^2 decreases as potential barrier height is reduced by the oxygen vacancy redistribution [Fig. 7(a-2)]. Figure 7(b-1) shows S_{IT}/I_T^2 vs f of the pristine and damaged FTJs operating in the HRS. In the HRS, its S_{IT}/I_T^2 increases when damage is given to FTJ. The result shows that the interface trap is increased by DC cycle stress, which increases the magnitude of $1/f$ noise. Interestingly, the behavior of S_{IT}/I_T^2 of the FTJs in LRS exhibits an opposite trend than that in HRS. The magnitude of $1/f$ noise is

Downloaded from http://pubs.aip.org/aip/apl/article-pdf/doi/10.1063/5.0140954/16821168/152901_1_5.0140954.pdf

Published under an exclusive license by AIP Publishing

decreased with the damage given to the FTJ, as shown in Fig. 7(b-2). If the increase in I_T of the FTJ in the LRS originates from the increase in bulk traps in the film (scenario 1), S_{IT}/I_T^2 should be increased after the damage is given. However, this scenario cannot explain the noise behavior of FTJ in the LRS. On the contrary, the noise behavior of FTJ in the LRS can be explained by scenario 2. The DC cycling-induced damage makes that oxygen vacancies migrate more easily, promoting the non-FE RS. Figure 7(c) shows S_{IT}/I_T^2 sampled at 100 Hz vs V_{PGM} of the pristine and damaged FTJs. The V_{TRANS} of the damaged FTJs (4.1 V) is lower than that of pristine devices (4.2 V). Using the LFN spectroscopy, we confirm that the DC cycling-induced damage enhances non-FE RS by facilitating the redistribution of oxygen vacancies.

We propose a method to examine two different RS mechanisms inherent to pure HfO_x FTJs using LFN spectroscopy: FE RS modulated by FE domain switching and non-FE RS modulated by oxygen vacancy redistribution. The dependence of S_{IT}/I_T^2 on V_{PGM} can be used to distinguish the RS mechanisms. It is revealed that the increase in T and N facilitates the oxygen vacancy redistribution in the HfO_x film, decreasing V_{TRANS}. This study paves the way for future advancements in the development of FTJs by introducing LFN spectroscopy as an effective method to examine the different RS mechanisms.

This research was supported in part by the National Research Foundation (NRF) funded by the Korean Ministry of Science and ICT under Grant No. 2022M3I7A2085479, in part by Samsung Research Funding & Incubation Center of Samsung Electronics under Project No. SRFC-TA2103-02, and in part by the BK21 FOUR program of the Education and Research Program for Future ICT Pioneers, Seoul National University in 2023.

AUTHOR DECLARATIONS

Conflict of Interest

The authors have no conflicts to disclose.

Author Contributions

Wonjun Shin and Ryun-Han Koo contributed equally to this work.

Wonjun Shin: Conceptualization (equal); Data curation (equal); Formal analysis (equal); Investigation (equal); Writing – original draft (equal). **Ryun-Han Koo:** Conceptualization (equal); Formal analysis (equal); Writing – original draft (equal). **Kyung Kyu Min:** Data curation (equal). **Been Kwak:** Formal analysis (equal). **Dongseok Kwon:** Data curation (equal). **Daewoong Kwon:** Formal analysis (equal); Funding acquisition (equal); Supervision (equal). **Jong-Ho Lee:** Supervision (equal); Writing – original draft (equal).

DATA AVAILABILITY

The data that support the findings of this study are available from the corresponding author upon reasonable request.

REFERENCES

[1] D. H. Looney, "Semiconductive translating device," US Patent 2791758 (1957).
[2] R. Zuleeg and H. H. Wieder, Solid-State Electron. **9**, 657–661 (1966).
[3] S.-Y. Wu, IEEE Trans. Electron Devices **21**, 499–504 (1974).
[4] S. Sakai and M. Takahashi, Materials **3**, 4950–4964 (2010).
[5] Z. Li, H. C. Thong, Y. F. Zhang, Z. Xu, Z. Zhou, Y. X. Liu, and K. Wang, Adv. Funct. Mater. **31**, 2005012 (2021).
[6] X. Zhou, K. Liu, Z. Yan, B. Xie, P. Fan, S. G. Chen, and H. Zhang, Ceramics Int. **48**(16), 23266 (2022).
[7] H. Mulaosmanovic, E. T. Breyer, S. Dünkel, S. Beyer, T. Mikolajick, and S. Slesazeck, Nanotechnology **32**, 502002 (2021).
[8] T. S. Böscke, J. Müller, D. Bräuhaus, U. Schröder, and U. Böttger, Appl. Phys. Lett. **99**, 102903 (2011).
[9] K. Mistry, in *IEEE International on Electron Devices Meeting* (IEEE, 2007), pp. 247–250.
[10] S. S. Cheema, D. Kwon, N. Shanker, R. Dos Reis, S. L. Hsu, J. Xiao, and S. Salahuddin, Nature **580**, 478–482 (2020).
[11] J. Yang, J. Zhou, J. Lu, Z. Luo, J. Yang, and L. Shen, Mater. Horiz. **9**, 1422–1430 (2022).
[12] H. Tan, G. Castro, J. Lyu, P. Loza-Alvarez, F. Sánchez, J. Fontcuberta, and I. Fina, Mater. Horiz. **9**, 2345–2352 (2022).
[13] S. Song, W. Ham, G. Park, W. Kho, J. Kim, H. Hwang, and S. E. Ahn, Adv. Mater. Technol. **7**, 2101323 (2022).
[14] X. Du, H. Sun, H. Wang, J. Li, Y. Yin, and X. Li, ACS Appl. Mater. Interfaces **14**, 1355–1361 (2022).
[15] K. K. Min, J. Yu, Y. Kim, J. H. Lee, D. Kwon, and B. G. Park, Nanotechnology **32**, 495203 (2021).
[16] Y. Kim, K. K. Min, J. Yu, D. Kwon, and B. G. Park, Semicond. Sci. Technol. **37**, 045001 (2022).
[17] B. Max, M. Pešić, S. Slesazeck, and T. Mikolajick, J. Appl. Phys. **123**, 134102 (2018).
[18] V. Mikheev, A. Chouprik, Y. Lebedinskii, S. Zarubin, A. M. Markeev, A. V. Zenkevich, and D. Negrov, Nanotechnology **31**, 215205 (2020).
[19] S. Ghosh, H. Surdi, F. Kargar, F. A. Koeck, S. Rumyantsev, S. Goodnick, and A. A. Balandin, Appl. Phys. Lett. **120**, 062103 (2022).
[20] J. K. Lee, S. Jung, J. Park, S. W. Chung, J. Sung Roh, S. J. Hong, and J. H. Lee, Appl. Phys. Lett. **101**, 103506 (2012).
[21] W. Shin, K. K. Min, J. H. Bae, J. Yim, D. Kwon, Y. Kim, and J. H. Lee, Nanoscale **14**, 2177–2185 (2022).
[22] W. Shin, R. H. Koo, K. K. Min, D. Kwon, J. J. Kim, D. Kwon, and J. H. Lee, IEEE Electron Device Lett. **44**, 345–348 (2023).
[23] R. H. Koo, W. Shin, K. K. Min, D. Kwon, D. H. Kim, J. J. Kim, and J. H. Lee, IEEE Electron Device Lett. **44**(1), 164–167 (2022).
[24] C. T. Angelis, J. Appl. Phys. **82**, 4095–4101 (1997).
[25] C. H. Park and J. H. Lee, Solid-State Electron. **69**, 85 (2012).
[26] X. Long, H. Tan, F. Sánchez, I. Fina, and J. Fontcuberta, ACS Appl. Electron. Mater. **5**(2), 740–747 (2023).
[27] G. Bersuker, D. C. Gilmer, D. Veksler, P. Kirsch, L. Vandelli, and A. Padovani, J. Appl. Phys. **110**(12), 124518 (2011).

Downloaded from http://pubs.aip.org/aip/apl/article-pdf/doi/10.1063/5.0140954/16821168/152901_1_5.0140954.pdf

Published under an exclusive license by AIP Publishing